

Studying the Process $\gamma d \rightarrow \pi^0 \eta d$ A. MARTÍNEZ TORRES^{a,b,*}, K.P. KHEMCHANDANI AND E. OSET^b^a*Universidade de Sao Paulo, Instituto de Fisica, C.P. 05389-970, Sao Paulo, Brazil*^b*Centro Mixto Universidad de Valencia-CSIC Institutos de Investigación de Paterna, Aptdo. 22085, 46071 Valencia, Spain*^c*Universidade Federal de São Paulo, C.P. 01302-907, São Paulo, Brazil*Doi: [10.12693/APhysPolA.142.378](https://doi.org/10.12693/APhysPolA.142.378)*e-mail: amartine@if.usp.br

In these proceedings, we present our recent results on the study of the process $\gamma d \rightarrow \pi^0 \eta d$, where the existence of a dibaryon in the ηd invariant mass distribution has been recently reported. As we will show, many of the relevant aspects observed in the experiment, such as the shift of the ηd and πd invariant mass distributions with respect to phase space, can be described with our model, where no dibaryon is formed. Instead, we consider the interaction of the γ with the nucleons forming the deuteron to proceed through $\gamma N \rightarrow \Delta(1700) \rightarrow \eta \Delta(1232) \rightarrow \eta \pi^0 N$, followed by the rescattering of the π and η with the other nucleon of the deuteron. Theoretical uncertainties related to different parameterizations of the deuteron wave function are investigated.

topics: dibaryons, meson-deuteron scattering

1. Introduction

In [1, 2], the $\gamma d \rightarrow \pi^0 \eta d$ reaction was investigated, and a clear shift with respect to phase space was observed in the ηd and πd invariant mass distributions. These distributions were fitted by considering a phenomenological model in which a dibaryon $D_{12}(2150)$ [$I(J^P) = 1(2^+)$] and a pole near the ηd threshold, with quantum numbers $I(J^P) = 0(1^-)$, are introduced in the $\pi^0 d$ and ηd invariant masses. By fitting the data, the mass and width of both dibaryons are obtained and found to be compatible with the corresponding values determined in the theoretical works claiming their existence [3–7]. Interestingly, the $D_{12}(2150)$ dibaryon found in [3, 4] has been recently explained in [8] as a $\Delta(1232)np$ triangle singularity of the reaction $pp \rightarrow \pi^+ d$, where $pp \rightarrow \Delta^+ p$, followed by $\Delta^+ \rightarrow \pi^+ n$, and the latter n together with the former p in the final state get bound in the form of a deuteron. Having this in mind, one can question whether the presence of a dibaryon in the ηd invariant mass distribution of the reaction $\gamma d \rightarrow \pi^0 \eta d$ is needed to explain the energy dependence observed in the experiment for the differential cross sections as a function of the ηd and $\pi^0 d$ invariant masses. It is our present topic of research.

The $\gamma d \rightarrow \pi^0 \eta d$ process was theoretically investigated in [9, 10], with the ηNN interaction being implemented considering different sets for the scattering length of ηN [5, 11]. However, the two models produce substantial differences in the respective ηd

and $\pi^0 d$ invariant mass distributions, and it is not clear if the existence of a dibaryon in the ηNN system is compatible with the ηd invariant mass distribution found in [2].

The existence of a η bound state has been a long-standing puzzle [12, 13] (for a review on the ηN interaction, we refer the reader to [14]). While theoretical calculations show that η bound states can appear for medium and heavy nuclei [15, 16], their widths are quite large compared to the corresponding binding, and no definite conclusion has been drawn about the existence of such η bound states in nuclei [17–19]. Even the existence of $\eta^3\text{He}$ and $\eta^4\text{He}$ bound states is still uncertain — while some models find a pole in the continuum, others suggest that deeper potentials than the current ones would be necessary in order to bind the η in ^3He or ^4He [20, 21]. In this respect, experimentally, the study of the $dd \rightarrow \eta^4\text{He} \rightarrow \pi^0 n^3\text{He}$, $\pi^- p^3\text{He}$ reactions do not find any evidence about the existence of $\eta^4\text{He}$ bound states [22, 23].

In view of the difficulties of finding η bound states in heavy nuclei, the search for an ηd bound state in nature does not seem promising. This means that some other dynamics should be responsible for the ηd and πd invariant mass distributions found in the $\gamma d \rightarrow \pi^0 \eta d$ reaction studied in [1, 2]. As we will show in this work, the formation of $\Delta(1700)$ from γN , together with its decay to $\eta \Delta(1232)$, are basically the main mechanisms involved in the process $\gamma d \rightarrow \pi^0 \eta d$.

2. Formalism

In our approach, the deuteron is considered to be a pn bound state with isospin $I = 0$ and orbital angular momentum $L = 0$, i.e.,

$$|d\rangle = \frac{1}{\sqrt{2}}(|pn\rangle - |np\rangle). \quad (1)$$

In this way, to describe the process $\gamma d \rightarrow \pi^0 \eta d$, we take that the photon can interact both with the p and n constituting the deuteron. Following [24, 25], the interaction of a photon with a nucleon to produce a $\eta\pi^0 N$ final state proceeds through the formation of the resonance $\Delta(1700)$. This state, which was found to be generated from the dynamics involved in the s -wave interaction between pseudoscalars and baryons from the decuplet in [26], couples mainly to the $\eta\Delta(1232)$ channel. The $\Delta(1232)$ decays to πN , getting in this way a $\pi\eta N$ final state from $\gamma N \rightarrow \Delta(1700) \rightarrow \eta\Delta(1232) \rightarrow \eta\pi N$ (see Fig. 1). In the impulse approximation, i.e., without considering the rescattering of the η and π^0 , we therefore have four mechanisms of getting $\gamma d \rightarrow \pi^0 \eta d$, as shown in Fig. 1.

Let us determine the different contributions to the amplitude in the impulse approximation. Following [25], the amplitude describing the vertex $\gamma N \rightarrow \Delta(1700)$ is given by

$$-it_{\gamma p \Delta^*} = g_{\gamma p \Delta^*} \mathbf{S}^\dagger \cdot \boldsymbol{\epsilon}, \quad (2)$$

where Δ^* represents $\Delta(1700)$, $\boldsymbol{\epsilon}$ is the polarization vector for the photon, and \mathbf{S} stands for the spin transition operator connecting states with spin 3/2 to 1/2. The value of the s -wave coupling $g_{\gamma p \Delta^*}$ in the preceding equation is taken to be 0.188 [25] (the Clebsch-Gordan coefficient $\sqrt{2/3}$ associated with the $\gamma N \rightarrow \Delta^*$ transition is already embedded on this value), which reproduces the experimental data on the radiative decay width of $\Delta(1700)$ [27]. It is

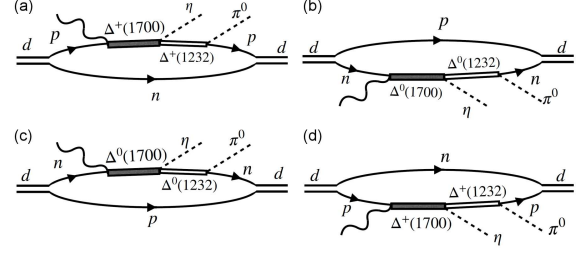


Fig. 1. Diagrams representing different contributions to the $\gamma d \rightarrow \pi^0 \eta d$ process within the impulse approximation, i.e., without considering the rescattering of the π and η coming from the decay of $\Delta(1700)$ and $\Delta(1232)$, respectively.

interesting to note that the amplitude in (2) is the same for proton as well as neutron since the photon must behave like an isovector particle in the vertex in order to produce $\Delta(1700)$, an isospin 3/2 baryon.

In the case of the vertex $\Delta(1700) \rightarrow \Delta(1232)\eta$, we can consider

$$-it_{\eta \Delta \Delta^*} = -ig_{\eta \Delta \Delta^*}, \quad (3)$$

with $g_{\eta \Delta \Delta^*} = 1.7 - i1.4$ [26]. Finally, for the $\Delta \rightarrow \pi N$ transition, following [8], we have

$$-it_{\Delta \rightarrow \pi N} = -\frac{f^*}{m_\pi} \mathbf{S} \cdot \mathbf{p}_\pi T^\lambda, \quad (4)$$

where $\mathbf{p}_\pi(m_\pi)$ is the momentum (mass) of the pion, $f^* = 2.13$, and $\mathbf{S}(T^\lambda)$ is the spin (isospin) transition operator acting on states with spin (isospin) 3/2 and taking them to 1/2. Note that the action of the isospin operator produces a factor $\sqrt{2/3}$ for the two types of $\Delta\pi N$ vertices appearing in the diagrams in Fig. 1, namely $\Delta^+ \pi^0 p$, $\Delta^0 \pi^0 n$.

In this way, we assume that

$$\begin{aligned} -it_{\text{impulse}} &= \frac{4}{\sqrt{6}} \int \frac{d^4 q}{(2\pi)^4} \left(-\frac{f^*}{m_\pi} \mathbf{S} \cdot \mathbf{p}_\pi \right) (g_{\gamma p \Delta^*} \mathbf{S}^\dagger \cdot \boldsymbol{\epsilon}) (-ig_{\eta \Delta \Delta^*}) \left[-ig_d \theta \left(q_{\text{max}} - |\mathbf{p}_N^{d_i}| \right) \right] \\ &\times \left[-ig_d \theta \left(q_{\text{max}} - |\mathbf{p}_N^{d_f}| \right) \right] \frac{M_N}{E_N(\mathbf{q})} \frac{i}{q^0 - E_N(\mathbf{q}) + i\epsilon} \frac{M_N}{E_N(\mathbf{p}_d - \mathbf{q})} \frac{i}{p_d^0 - q^0 - E_N(\mathbf{p}_d - \mathbf{q}) + i\epsilon} \\ &\times \frac{M_{\Delta^*}}{E_{\Delta^*}(\mathbf{p}_d - \mathbf{q} + \mathbf{k})} \frac{i}{p_d^0 - q^0 + k^0 - E_{\Delta^*}(\mathbf{p}_d - \mathbf{q} + \mathbf{k}) + i\epsilon} \\ &\times \frac{M_\Delta}{E_\Delta(\mathbf{p}_d - \mathbf{q} + \mathbf{k} - \mathbf{p}_\eta)} \frac{i}{p_d^0 - q^0 + k^0 - p_\eta^0 - E_\Delta(\mathbf{p}_d - \mathbf{q} + \mathbf{k} - \mathbf{p}_\eta) + i\epsilon} \\ &\times \frac{M_N}{E_N(\mathbf{p}_d - \mathbf{q} + \mathbf{k} - \mathbf{p}_\eta - \mathbf{p}_\pi)} \frac{i}{p_d^0 - q^0 + k^0 - p_\eta^0 - p_\pi^0 - E_N(\mathbf{p}_d - \mathbf{q} + \mathbf{k} - \mathbf{p}_\eta - \mathbf{p}_\pi) + i\epsilon}, \end{aligned} \quad (5)$$

where p_d , k , p_η , and p_π represent, respectively, the four-momentum of: the deuteron in the initial state, the initial photon, and the η and π^0 in the final state. In (5), the four-momentum q is related to the nucleon inside the deuteron, which

does not interact with the photon in Fig. 1. The constant g_d in (5) is the $d \leftrightarrow pn$ coupling, with a value of $(2\pi)^{3/2} 2.68 \times 10^{-3} \text{ MeV}^{-1/2}$ [8], while $\mathbf{p}_N^{d_i}(\mathbf{p}_N^{d_f})$ represents the linear momentum of the

nucleon in the rest frame of the deuteron in the initial (final) state. In (5), q_{\max} is a cut-off for the momentum of the nucleons in the rest frame of the deuteron. Within non-relativistic kinematics, which is appropriate for the process, we can write

$$\mathbf{p}_N^{d_i} = \frac{\mathbf{p}_d}{2} - \mathbf{q}, \quad \mathbf{p}_N^{d_f} = \frac{\mathbf{p}_d + \mathbf{k} - \mathbf{p}_\eta - \mathbf{p}_\pi}{2} - \mathbf{q}. \quad (6)$$

Next, we perform the dq^0 integration of (5) by means of Cauchy's theorem, and we find

$$\begin{aligned} -i t_{\text{impulse}} = & -2i \sqrt{\frac{2}{3}} \int \frac{d^3 q}{(2\pi)^3} \left(\frac{f^*}{m_\pi} \mathbf{S} \cdot \mathbf{p}_\pi \right) (g_{\gamma p \Delta^*} \mathbf{S}^\dagger \cdot \boldsymbol{\epsilon}) (g_{\eta \Delta \Delta^*}) \left[g_d \theta \left(q_{\max} - \left| \frac{\mathbf{p}_d}{2} - \mathbf{q} \right| \right) \right] \\ & \times \left[g_d \theta \left(q_{\max} - \left| \frac{\mathbf{p}_d + \mathbf{k} - \mathbf{p}_\eta - \mathbf{p}_\pi}{2} - \mathbf{q} \right| \right) \right] \frac{M_N}{E_N(\mathbf{q})} \frac{M_N}{E_N(\mathbf{p}_d - \mathbf{q})} \frac{1}{p_d^0 - E_N(\mathbf{q}) - E_N(\mathbf{p}_d - \mathbf{q}) + i\epsilon} \\ & \times \frac{M_{\Delta^*}}{E_{\Delta^*}(\mathbf{p}_d - \mathbf{q} + \mathbf{k})} \frac{1}{p_d^0 - E_N(\mathbf{q}) + k^0 - E_{\Delta^*}(\mathbf{p}_d - \mathbf{q} + \mathbf{k}) + i\epsilon} \\ & \times \frac{M_\Delta}{E_\Delta(\mathbf{p}_d - \mathbf{q} + \mathbf{k} - \mathbf{p}_\eta)} \frac{1}{p_d^0 - E_N(\mathbf{q}) + k^0 - p_\eta^0 - E_\Delta(\mathbf{p}_d - \mathbf{q} + \mathbf{k} - \mathbf{p}_\eta) + i\epsilon} \\ & \times \frac{M_N}{E_N(\mathbf{p}_d - \mathbf{q} + \mathbf{k} - \mathbf{p}_\eta - \mathbf{p}_\pi)} \frac{1}{p_d^0 - E_N(\mathbf{q}) + k^0 - p_\eta^0 - p_\pi^0 - E_N(\mathbf{p}_d - \mathbf{q} + \mathbf{k} - \mathbf{p}_\eta - \mathbf{p}_\pi) + i\epsilon}. \end{aligned} \quad (7)$$

Since the reaction we are investigating involves deuterons in the initial and final states, it is convenient to introduce the corresponding wave function ψ of the deuteron for a better comparison with the data. To do this, following [8, 28], we can replace

$$\begin{aligned} g_d \theta \left(q_{\max} - \left| \frac{\mathbf{p}_d}{2} - \mathbf{q} \right| \right) \frac{M_N}{E_N(\mathbf{q})} \frac{M_N}{E_N(\mathbf{p}_d - \mathbf{q})} \\ \times \frac{1}{p_d^0 - E_N(\mathbf{q}) - E_N(\mathbf{p}_d - \mathbf{q}) + i\epsilon} \end{aligned} \quad (8)$$

by $-(2\pi)^{3/2} \psi(\frac{1}{2}\mathbf{p}_d - \mathbf{q})$. Note that in our case, the value g_d used is compatible with the following normalization of the deuteron wave function

$$\int d^3 q |\psi(\mathbf{q})|^2 = 1. \quad (9)$$

Similarly, we can substitute the other combination of g_d , θ -function, and two-nucleon Green's function present in the amplitude given by (7) by a $-(2\pi)^{3/2} \psi(\frac{1}{2}(\mathbf{p}_d + \mathbf{k} - \mathbf{p}_\eta - \mathbf{p}_\pi) - \mathbf{q})$. This way, we can rewrite (7) as

$$\begin{aligned} t_{\text{impulse}} = & 2\sqrt{\frac{2}{3}} g_{\gamma p \Delta^*} g_{\eta \Delta \Delta^*} \frac{f^*}{m_\pi} M_\Delta M_{\Delta^*} \int \frac{d^3 q}{(2\pi)^3} \frac{(\mathbf{S} \cdot \mathbf{p}_\pi)(\mathbf{S}^\dagger \cdot \boldsymbol{\epsilon})}{[E_{\Delta^*}(\mathbf{p}_d - \mathbf{q} + \mathbf{k})][E_\Delta(\mathbf{p}_d - \mathbf{q} + \mathbf{k} - \mathbf{p}_\eta)]} \\ & \times \frac{1}{p_d^0 - E_N(\mathbf{q}) + k^0 - E_{\Delta^*}(\mathbf{p}_d - \mathbf{q} + \mathbf{k}) + i\epsilon} \frac{1}{p_d^0 - E_N(\mathbf{q}) + k^0 - p_\eta^0 - E_\Delta(\mathbf{p}_d - \mathbf{q} + \mathbf{k} - \mathbf{p}_\eta) + i\epsilon} \\ & \times (2\pi)^3 \psi \left(\frac{\mathbf{p}_d}{2} - \mathbf{q} \right) \psi \left(\frac{\mathbf{p}_d + \mathbf{k} - \mathbf{p}_\eta - \mathbf{p}_\pi}{2} - \mathbf{q} \right). \end{aligned} \quad (10)$$

To estimate theoretical uncertainties, we will use different well-known parameterizations for the deuteron wave function, such as those of [29–32].

Next, (10) has the spin structure $(\mathbf{S} \cdot \mathbf{p}_\pi)(\mathbf{S}^\dagger \cdot \boldsymbol{\epsilon})$, and we need to evaluate the different spin transitions considering the two possible polarizations of the photon and the different spin projections of the deuteron. To do this, first, we choose the photon momentum to be parallel to the z -axis, such that $\mathbf{k} = (0, 0, |\mathbf{k}|)$. In this way, the polarization vectors of the photon are given by $\boldsymbol{\epsilon}_1 = (1, 0, 0)$, $\boldsymbol{\epsilon}_2 = (0, 1, 0)$. Then, we make use of the useful property $\sum_{\text{polar.}} S_i S_j^\dagger = \frac{2}{3} \delta_{ij} - \frac{i}{3} \epsilon_{ijk} \sigma_k$ and the fact that Δ is produced at the vertex $\Delta^* \rightarrow \Delta\eta$, which

implies that the spin projections of Δ^* and Δ always coincide, i.e., $m_{\Delta^*} = m_\Delta$. Then we can write

$$\begin{aligned} (\mathbf{S} \cdot \mathbf{p}_\pi)(\mathbf{S}^\dagger \cdot \boldsymbol{\epsilon}) = & \sum_{m_\Delta} p_{\pi_i} \epsilon_j S_i |m_\Delta\rangle \langle m_\Delta| S_j^\dagger = \\ & \frac{2}{3} \mathbf{p}_\pi \cdot \boldsymbol{\epsilon} - \frac{i}{3} \epsilon_{ijk} p_{\pi_i} \epsilon_j \sigma_k. \end{aligned} \quad (11)$$

By means of (11), we can now evaluate the corresponding matrix elements for the different polarization vectors of the incident photon and the spin projections of the nucleons forming the deuteron. Let us denote these matrix elements by $W_{\mu, \mu'}^\lambda$, where the indices $\mu, \mu' = -1, 0, 1$ represent, respectively, the spin projections $\downarrow\downarrow, \uparrow\downarrow + \downarrow\uparrow$, and $\uparrow\uparrow$ of the nucleons

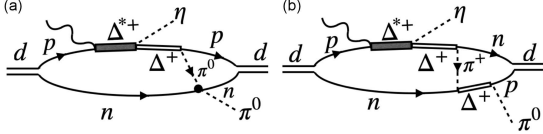


Fig. 2. Some of the diagrams representing contributions to the rescattering of the pion in the intermediate state in s - (a) and p -waves (b). The thick dot stands for the s -wave $\pi N \rightarrow \pi N$ interaction. There are eight diagrams in total concerning the rescattering of a pion in s -wave and another eight diagrams for the rescattering of a pion in p -wave. For the full set of diagrams, we refer the reader to [33].

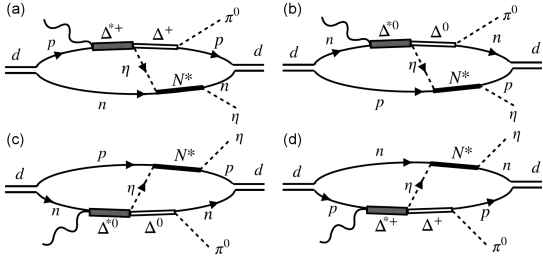


Fig. 3. Diagrams representing contributions to the s -wave rescattering of an η with one of the nucleons of the deuteron.

in the deuteron, and $\lambda = 1, 2$ represents the two possible polarization vectors of the photon. In this way, we have, for example,

$$\begin{aligned} W_{1,1}^\lambda &= \langle \uparrow\uparrow | \mathbf{S} \cdot \mathbf{p}_\pi \mathbf{S}^\dagger \cdot \boldsymbol{\epsilon}_\lambda | \uparrow\uparrow \rangle, \\ W_{1,0}^\lambda &= \left\langle \frac{1}{\sqrt{2}} (\uparrow\downarrow + \downarrow\uparrow) | \mathbf{S} \cdot \mathbf{p}_\pi \mathbf{S}^\dagger \cdot \boldsymbol{\epsilon}_\lambda | \uparrow\uparrow \right\rangle, \\ W_{1,-1}^\lambda &= \langle \downarrow\downarrow | \mathbf{S} \cdot \mathbf{p}_\pi \mathbf{S}^\dagger \cdot \boldsymbol{\epsilon}_\lambda | \uparrow\uparrow \rangle. \end{aligned} \quad (12)$$

Thus, the amplitude in the impulse approximation obtained in (10) depends on the spin projections of the deuteron in the initial (μ) and final (μ') states, as well as on the transverse polarization of the photon (λ). It is then convenient to use the notation $t_{\mu,\mu'}^\lambda$. In Table I, we list all $W_{\mu,\mu'}^\lambda$ matrix elements obtained in the impulse approximation.

After evaluating the amplitude in the impulse approximation, the next contribution to the process $\gamma d \rightarrow \pi^0 \eta d$ in our approach corresponds to the rescattering of π and η . Note that π can rescatter with one of the nucleons of the deuteron in the s -wave as well as in the p -wave, i.e., relative orbital angular momentum $l = 0, 1$ (we present some of the corresponding diagrams in Fig. 2 [33]). In the former case, we follow the approach of [34] to determine the $\pi N \rightarrow \pi N$ amplitude in s -wave, while in the latter case, $\Delta(1232)$ is exchanged, with the $\Delta \rightarrow \pi N$ vertex being described by the amplitude in (4).

In the case of the rescattering of the η with one of the nucleons of the deuteron, the $N^*(1535)$ can be generated in s -wave. As shown in [35], this latter

state couples mainly to $K\Sigma$ and ηN , with the coupling $g_{\eta NN^*(1535)} = 1.46 - i0.43$, and we have the contributions shown in Fig. 3.

Following the same methodology to get the contribution in the impulse approximation, we can determine the amplitudes for the rescattering of a pion in s - and p -waves as well as that related to the rescattering of an η in the s -wave. For the explicit expressions as well as for more details on the calculations, we refer the reader to [33].

Finally, we implement in our approach the unstable nature of states like $\Delta^*(1700)$, $\Delta(1232)$, and $N^*(1535)$ by replacing $E_R - i\epsilon$ with $E_R - i\Gamma_R/2$ in the different amplitudes, where R stands for a resonance/unstable state. In the case of $\Delta(1232)$, we consider an energy-dependent width

$$\Gamma_\Delta(M_{\Delta inv}) = \Gamma_\Delta \frac{M_\Delta}{M_{\Delta inv}} \left(\frac{q_\pi}{q_{\pi on}} \right)^3, \quad (13)$$

where q_π and $q_{\pi on}$ are defined as

$$\begin{aligned} q_\pi &= \frac{\sqrt{\lambda} (M_{\Delta inv}^2, M_N^2, m_\pi^2)}{2M_{\Delta inv}}, \\ q_{\pi on} &= \frac{\sqrt{\lambda} (M_\Delta^2, M_N^2, m_\pi^2)}{2M_\Delta}, \end{aligned} \quad (14)$$

with

$$M_{\Delta inv}^2 = E_\Delta^2 - |\mathbf{p}_\Delta|^2. \quad (15)$$

3. Results and discussions

Using the amplitudes discussed in the previous section, we can determine the invariant mass distributions for ηd and $\pi^0 d$ in the final state as

$$\begin{aligned} \frac{d\sigma}{dM_{\eta d}} &= \frac{M_d^2}{8|\mathbf{k}|s} \frac{|\mathbf{p}_\pi||\mathbf{p}_\eta^{R\eta d}|}{(2\pi)^4} \int d\cos(\theta_\pi) \int d\Omega_\eta^{R\eta d} \\ &\times \overline{\sum_{\mu,\lambda} \sum_{\mu'}} |t_{\mu,\mu'}^\lambda|^2, \end{aligned} \quad (16)$$

$$\begin{aligned} \frac{d\sigma}{dM_{\pi^0 d}} &= \frac{M_d^2}{8|\mathbf{k}|s} \frac{|\mathbf{p}_\eta||\mathbf{p}_\pi^{R\pi d}|}{(2\pi)^4} \int d\cos(\theta_\eta) \int d\Omega_\pi^{R\pi d} \\ &\times \overline{\sum_{\mu,\lambda} \sum_{\mu'}} |t_{\mu,\mu'}^\lambda|^2, \end{aligned} \quad (17)$$

where the summation signs represent the sum over the polarizations of the particles in the initial and final states, with the bar over the sign indicating averaging over the initial state polarization. In (16) and (17), s is the standard Mandelstam variable, \mathbf{p}_π (\mathbf{p}_η) is the pion (eta) momentum in the global center of mass frame, and $\mathbf{p}_\eta^{R\eta d}$ ($\mathbf{p}_\pi^{R\pi d}$) denotes the eta (pion) momentum in the rest frame of ηd (πd). The variable $\Omega_\eta^{R\eta d}$ ($\Omega_\pi^{R\pi d}$) in (16) and in (17) is the solid angle of η (π) in the ηd (πd) rest frame. Note that we calculate the amplitudes in the global center of mass frame, i.e., $\mathbf{p}_d + \mathbf{k} = 0$, and $p_d^0 + k^0$ is taken as \sqrt{s} . Thus, we must boost $\mathbf{p}_\pi^{R\pi d}$ and $\mathbf{p}_\eta^{R\eta d}$ to the global center of mass frame. The expressions for the boosted η and \mathbf{p}_π momenta can be found in [33].

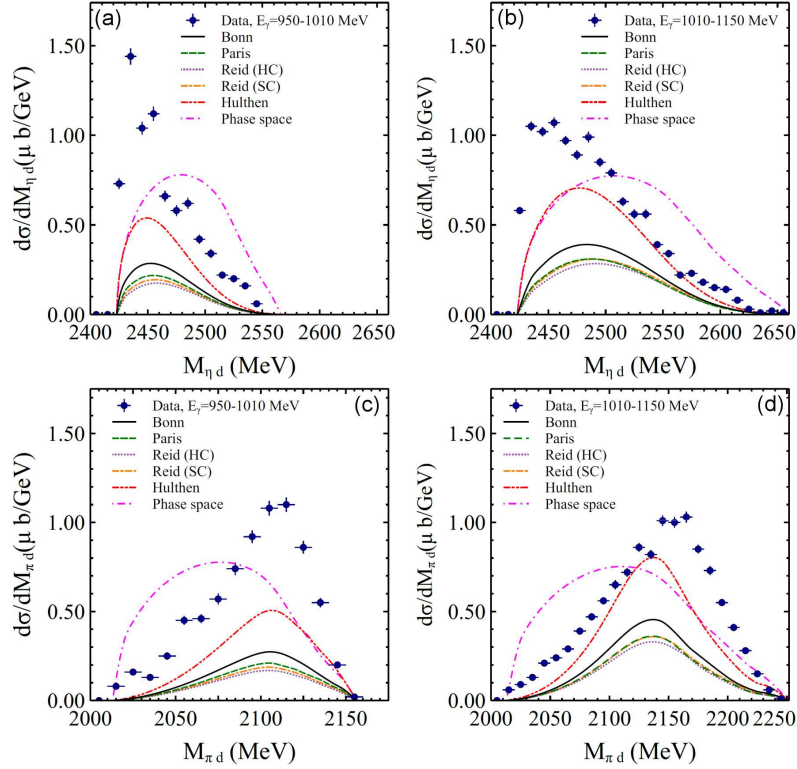


Fig. 4. Differential cross sections obtained in the impulse approximation as a function of the ηd (panels (a) and (b)) and $\pi^0 d$ (panels (c) and (d)) invariant masses. Panels (a) and (c) show average cross sections for the beam energy range $E_\gamma = 950$ – 1010 MeV, while panels (b) and (d) — for $E_\gamma = 1010$ – 1150 MeV. Experimental data, shown as filled circles, are taken from [1]. The deuteron wave functions considered in the calculations are based on the following parameterizations for the NN potentials: Bonn [29], Paris [30], Reidt Hard-Core (HC) and Soft-Core (SC) [31] and Hulthén [32].

TABLE I

Spin transition elements $W_{\mu,\mu'}^\lambda$. The subscripts μ and μ' are related to the polarizations of the deuteron in the initial and final states. Note that $W_{\mu',\mu}^\lambda$ is the negative of the complex conjugate of $W_{\mu,\mu'}^\lambda$, thus, it suffices to list any one of them.

μ	μ'	$W_{\mu,\mu'}^\lambda$
1	1	$\frac{2}{3}\mathbf{p}_\pi \cdot \boldsymbol{\epsilon}_\lambda - \frac{i}{3}(p_{\pi_x}\epsilon_{\lambda_y} - p_{\pi_y}\epsilon_{\lambda_x})$
1	0	$-\frac{i}{3\sqrt{2}}(-p_{\pi_z}\epsilon_{\lambda_y} + ip_{\pi_z}\epsilon_{\lambda_x})$
1	-1	0
0	0	$\frac{2}{3}\mathbf{p}_\pi \cdot \boldsymbol{\epsilon}_\lambda$
0	-1	$-\frac{i}{3\sqrt{2}}(-p_{\pi_z}\epsilon_{\lambda_y} + ip_{\pi_z}\epsilon_{\lambda_x})$
-1	-1	$\frac{2}{3}\mathbf{p}_\pi \cdot \boldsymbol{\epsilon}_\lambda + \frac{i}{3}(p_{\pi_x}\epsilon_{\lambda_y} - p_{\pi_y}\epsilon_{\lambda_x})$

Let us now discuss the results obtained. We start with the invariant mass distributions found considering the impulse approximation. The results obtained are shown in Fig. 4. In the experiment, two different sets of photon beam energies are considered, 950–1010 MeV and 1010–1150 MeV. Thus, to compare with the experimental data, we need to calculate the ηd and $\pi^0 d$ mass distributions for

different energies between 950–1010 MeV as well as between 1010–1150 MeV and determine the average values. In particular, we consider the energies 950, 980, and 1010 MeV for the first energy range and 1010, 1050, 1100, and 1150 MeV for the second energy range. In Fig. 4, panels (a) and (c) represent the results obtained averaging the curves found for $E_\gamma = 950$ – 1010 MeV, and panels (b) and (d) — the results obtained averaging the curves found for $E_\gamma = 1010$ – 1150 MeV. Panels (a) and (b) are related to the results obtained for the ηd invariant mass distribution, while (c) and (d) — to the results obtained for the $\pi^0 d$ invariant mass distribution. The different lines shown in Fig. 4 correspond to the results obtained with different parameterizations of the deuteron wave function. As can be seen, the shift, with respect to phase space shown by the data in [1], on the differential cross section can be reproduced with the impulse approximation, and it is a consequence of the dynamics considered (see Fig. 1). Indeed, the mechanism in Fig. 1 favors the π^0 to go with as high energy as possible to place the $\Delta(1232)$ on-shell. This leaves less energy for the η , and the ηd invariant mass becomes smaller. Conversely, the π^0 goes out with larger energy than expected from phase space leading to a πd invariant mass bigger than the phase space contribution.

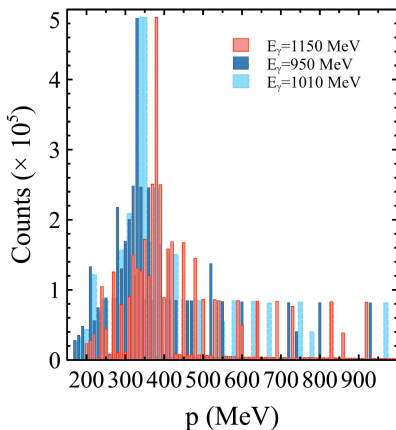


Fig. 5. Accumulation of events satisfying the condition in (18) for values of q_{\max} in the range 0–1000 MeV.

Note, however, that the magnitude of the distributions shown in Fig. 4 is substantially affected by the choice of the wave function parameterization considered in the calculations. Such differences are related to the typical momentum values of the deuteron in the reaction considered. Indeed, as can be seen in Fig. 5, the deuteron wave function gets determined most frequently in the momentum range 300–400 MeV for different values of the photon energy.

This result has been found by generating random numbers when calculating the phase-space integration for the differential cross sections. Then, by collecting the events which satisfy the condition

$$\theta\left(q_{\max} - \left|\frac{\mathbf{p}_d}{2} - \mathbf{q}\right|\right) \times \theta\left(q_{\max} - \left|\frac{\mathbf{p}_d + \mathbf{k} - \mathbf{p}_\eta - \mathbf{p}_\pi}{2} - \mathbf{q}\right|\right) = 1, \quad (18)$$

while changing q_{\max} from 10 to 1000 MeV, in steps of 10 MeV, we can define R_i as the number found for the i -th value of q_{\max} . In this way, the difference $R_{i+1} - R_i$ provides the fraction of events where either $|\frac{1}{2}\mathbf{p}_d - \mathbf{q}|$ or $|\frac{1}{2}(\mathbf{p}_d + \mathbf{k} - \mathbf{p}_\eta - \mathbf{p}_\pi) - \mathbf{q}|$ are between q_{\max} and $q_{\max} + 10$ MeV.

Considering the momentum region 300–400 MeV, as can be seen in Fig. 6, different parameterizations of the deuteron wave functions produce substantial differences precisely in this momentum region. The different wave functions of the deuteron are related to different parameterizations of the NN potential, parameterizations which are based on meson exchange potentials. Therefore, they should be expected to work at distances where the nucleons do not overlap. However, this should not be the case for the momentum of the deuteron ranging between 300–400 MeV. Then the NN scattering models of [29–32] cannot provide precise descriptions for the deuteron wave function in the momentum range needed to study the reaction $\gamma d \rightarrow \pi^0 \eta d$.

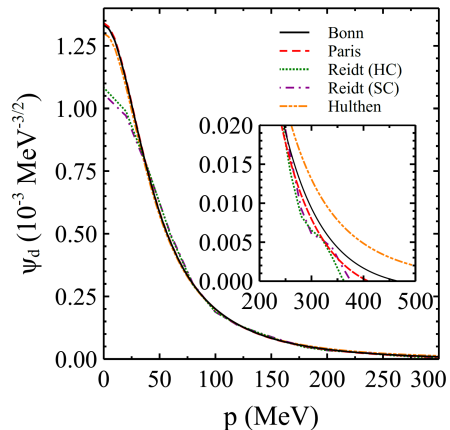


Fig. 6. Deuteron wave functions based on the following parameterizations for the NN potentials: Bonn [29], Paris [30], Reidt Hard-Core (HC) and Soft-Core (SC) [31] and Hulthén [32].

That being said, it is important to know if the rescattering mechanisms shown in Figs. 2 and 3 are relevant for describing the data on $\gamma d \rightarrow \pi^0 \eta d$. We show the ηd and $\pi^0 d$ distributions in Fig. 7 obtained with the Bonn [29] and Hulthén models [32] for the deuteron wave function to illustrate the uncertainty related to the choice of the deuteron wave function parameterization.

As can be seen in Fig. 7, independently of the parameterization of the deuteron wave function, the effect of rescattering is relevant and leads to an increase in the strength of the mass distribution of about 50%. We also find that the rescattering of a pion in p -wave, through the mechanism $\pi N \rightarrow \Delta(1232) \rightarrow \pi N$, produces the dominant contribution. The increase of the magnitude obtained for the distributions when the rescattering is implemented can be explained by the fact that the rescattering mechanism in this case helps to share the momentum transfer between the two nucleons of the deuteron and involves the deuteron wave function at smaller momenta, where it is bigger (see Fig. 6). Note, however, that even with the increase in the magnitude produced by the rescattering, the magnitude obtained for the differential cross sections for $E_\gamma = 950$ –1010 MeV is still smaller than that of the experimental data.

To finalize this section, in Fig. 8, we show the results obtained on the angular distributions with the impulse approximation and with the inclusion of the rescattering processes. Since, as can be seen in Fig. 7, the contribution from the η rescattering in s -wave is not significant, it is sufficient for comparing with the data to consider the effects from the rescattering of a pion. The uncertainties associated with the parameterizations of the deuteron wave function (based on Bonn and Hulthén potentials) are also shown. As can be seen in Fig. 8, the differential cross sections are underestimated at the forward angles, while at backward angles, they are

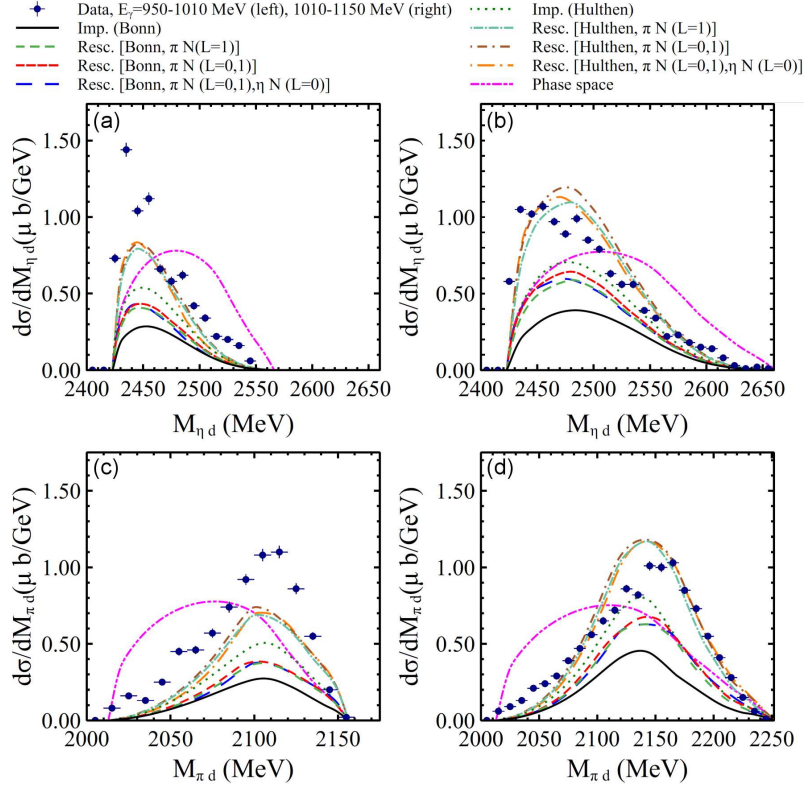


Fig. 7. Differential cross sections as a function of the ηd (panels (a) and (b)) and $\pi^0 d$ ((c) and (d)) invariant masses, as obtained in the impulse approximation and by considering the rescattering of π in p -wave (orbital angular momentum $L = 1$), as well as in s -wave ($L = 0$), and the rescattering of η in s -wave ($L = 0$). Panels (a) and (c) represent average cross sections for the beam energy range $E_\gamma = 950$ – 1010 MeV, while panels (b) and (d) — for ($E_\gamma = 1010$ – 1150 MeV). The experimental data, shown as filled circles, are taken from [1].

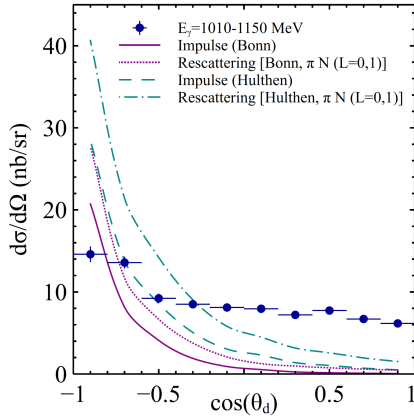


Fig. 8. Differential cross sections as a function of the polar angle of the outgoing deuteron. The experimental data are taken from [2].

overestimated. Similar results have been found in [9, 10], and we do not have an explanation for such discrepancies, particularly since the forward angle requires large deuteron momenta, and even the large increase produced by the Hulthén wave function is clearly insufficient to reach the experimental values in the forward region.

4. Conclusions

In these proceedings, we have shown the results found for the ηd and $\pi^0 d$ mass distributions in the process $\gamma d \rightarrow \pi^0 \eta d$. Our description of the reaction is based on a realistic model for the $\gamma N \rightarrow \pi^0 \eta N$ process, where first γN couples to the resonance $\Delta(1700)$, which decays to $\eta \Delta(1232)$, and the subsequent decay of $\Delta(1232)$ to πN produces the final state $\pi^0 \eta d$. Once a π and an η are produced, we can also have the rescattering of these particles with the nucleons of the deuteron. The needed couplings to determine all these contributions, such as that of $\Delta(1700) \rightarrow \eta \Delta(1232)$, are provided by previous theoretical studies. Thus, predictions for observables of the $\gamma d \rightarrow \pi^0 \eta d$ reaction are obtained without fitting to the data.

As we have shown, the shift of the data with respect to phase space can be explained with the above-mentioned dynamics, and there is no need to consider the existence of dibaryons. Particularly relevant for describing the data is the contribution from the rescattering of a pion in p -wave, which increases the magnitude found for the differential cross sections with the amplitudes in the impulse approximation considerably, (by as much as 50%).

We have also shown that the reaction investigated involves large momenta of the deuteron, in a region of momenta, where the nucleons inside the deuteron clearly overlap, and it is difficult to give precise values of the deuteron wave function. This is the reason why we used different parameterizations for the deuteron wave function, which helped us quantify the uncertainties of the theoretical calculation, and they were found to be sizable.

With the mechanisms considered, the model predicts an angular distribution clearly peaking at backward angles. This result is in clear conflict with the experimental data, which correspond to a much flatter distribution.

Acknowledgments

This work is partly supported by the Spanish Ministerio de Economía y Competitividad and European FEDER funds under Contracts No. PID2020-112777GB-I00, and by Generalitat Valenciana under contract PROMETEO/2020/023. This project has received funding from the European Unions 10 Horizon 2020 research and innovation programme under grant agreement No. 824093 for the “STRONG-2020” project. K.P.K and A.M.T gratefully acknowledge the travel support from the above mentioned projects. K.P.K and A.M.T also thank the financial support provided by Fundação de Amparo à Pesquisa do Estado de São Paulo (FAPESP), processos n° 2019/17149-3 and 2019/16924-3 and the Conselho Nacional de Desenvolvimento Científico e Tecnológico (CNPq), grants no. 305526/2019-7 and 303945/2019-2, which has facilitated the numerical calculations presented in this work.

References

- [1] T. Ishikawa, H. Fujimura, H. Fukasawa et al., *Phys. Rev. C* **104**, L052201 (2021).
- [2] T. Ishikawa, A. Fix, H. Fujimura et al., *Phys. Rev. C* **105**, 045201 (2022).
- [3] A. Gal, H. Garcilazo, *Nucl. Phys. A* **928**, 73 (2014).
- [4] O. Kolesnikov, A. Fix, *J. Phys. G* **48**, 085101 (2021).
- [5] A.M. Green, S. Wycech, *Phys. Rev. C* **55**, R2167 (1997).
- [6] A. Fix, H. Arenhovel, *Eur. Phys. J. A* **9**, 119 (2000).
- [7] N. Barnea, E. Friedman, A. Gal, *Phys. Lett. B* **747**, 345 (2015).
- [8] N. Ikeno, R. Molina, E. Oset, *Phys. Rev. C* **104**, 014614 (2021).
- [9] M. Egorov, A. Fix, *Phys. Rev. C* **88**, 054611 (2013).
- [10] M. Egorov, *Phys. Rev. C* **101**, 065205 (2020).
- [11] C. Wilkin, *Phys. Rev. C* **47**, R938 (1993).
- [12] R.S. Bhalerao, L.C. Liu, *Phys. Rev. Lett.* **54**, 865 (1985).
- [13] Q. Haider, L.C. Liu, *Phys. Lett. B* **172**, 257 (1986).
- [14] S.D. Bass, P. Moskal, *Rev. Mod. Phys.* **91**, 015003 (2019).
- [15] H.C. Chiang, E. Oset, L.C. Liu, *Phys. Rev. C* **44**, 738 (1991).
- [16] T. Inoue, E. Oset, *Nucl. Phys. A* **710**, 354 (2002).
- [17] H. Machner, *J. Phys. G* **42**, 043001 (2015).
- [18] N.G. Kelkar, K.P. Khemchandani, N.J. Upadhyay, B.K. Jain, *Rep. Prog. Phys.* **76**, 066301 (2013).
- [19] V. Metag, M. Nanova, E.Y. Paryev, *Prog. Part. Nucl. Phys.* **97**, 199 (2017).
- [20] J.-J. Xie, W.-H. Liang, E. Oset, P. Moskal, M. Skurzok, C. Wilkin, *Phys. Rev. C* **95**, 015202 (2017).
- [21] J.-J. Xie, W.-H. Liang, E. Oset, *Eur. Phys. J. A* **55**, 6 (2019).
- [22] P. Adlarson, W. Augustyniak, W. Bardan (WASA-at-COSY Collaboration) et al., *Phys. Rev. C* **87**, 035204 (2013).
- [23] P. Adlarson P. Adlarson, W. Augustyniak, W. Bardan et al., *Nucl. Phys. A* **959**, 102 (2017).
- [24] M. Doring, E. Oset, D. Strottman, *Phys. Rev. C* **73**, 045209 (2006).
- [25] V.R. Debastiani, S. Sakai, E. Oset, *Phys. Rev. C* **96**, 025201 (2017).
- [26] S. Sarkar, E. Oset, M.J. Vicente Vacas, *Nucl. Phys. A* **750**, 294 (2005); Erratum: *Nucl. Phys. A* **780**, 90 (2006).
- [27] P.A. Zyla, R.M. Barnett, J. Beringer et al. (Particle Data Group), *Prog. Theor. Exper. Phys.* **2020**, 083C01 (2020).
- [28] D. Gamermann, J. Nieves, E. Oset, E. Ruiz Arriola, *Phys. Rev. D* **81**, 014029 (2010).
- [29] R. Machleidt, *Phys. Rev. C* **63**, 024001 (2001).
- [30] M. Lacombe, B. Loiseau, R. Vinh Mau, J. Cote, P. Pires, R. de Tourreil, *Phys. Lett. B* **101**, 139 (1981).
- [31] R.V. Reid, Jr., *Annals Phys.* **50**, 411 (1968).
- [32] R.J. Adler, T.K. Das, A. Ferraz Filho, *Phys. Rev. C* **16**, 1231 (1977).
- [33] A. Martinez Torres, K.P. Khemchandani, E. Oset, [arXiv:2205.00948](https://arxiv.org/abs/2205.00948) (2022).
- [34] E. Oset, M.J. Vicente-Vacas, *Nucl. Phys. A* **446**, 584 (1985).
- [35] T. Inoue, E. Oset, M.J. Vicente Vacas, *Phys. Rev. C* **65**, 035204 (2002).